ory of the Navier-Stokes Equations—Vol.
York (1994)
odynamischen Grundgleichungen. Math.
ılarity of suitable weak solutions to the
Fluid Mech. 1(4), 356–387 (1999)
x emplissant l'espace. Acta Math. 63,
berg theorem. Comm. Pure Appl. Math.
er-Stokes equations. Pacific J. Math. 66,
kes equations. Comm. Math. Phys. 55,
oluitons of the Navier-Stokes equations
1), 147–178 (2003); trans. from Algebra
n. Lecture Notes Mathematics, Vol. 268.
e Laplacian in Bounded and Unbounded
ies, Vol. 360. Addison Wesley Longman
entary Functional Analytic Approach.
essure of weak solutions of the Navier-
986)
okes equations. Commun. Anal. Geom.
solutions to Navier-Stokes equations.
14(5–6), 735–785 (2007)
ions of non-stationary motion of non-
y. J. Math. Fluid Mech. 9(1), 104–138
enberg theorem. Banach Center Publ.:
008)

An In Vitro Device for Evaluation of Cellular Response to Flows Found at the Apex of Arterial Bifurcations

Zijing Zeng, Bong Jae Chung, Michael Durka, and Anne M. Robertson

Abstract Intracranial aneurysms (ICA) are abnormal dilations of the cerebral arteries, most commonly located at the apices of bifurcations. The ability of the arterial wall, particularly the endothelial cells forming the inner lining of the wall, to respond appropriately to hemodynamic stresses is critical to arterial health. ICA initiation is believed to be caused by a breakdown in this homeostatic mechanism leading to wall degradation. Due to the complex nature of this process, there is a need for both controlled in vitro and in vivo studies. Chung et al. developed an in vitro chamber for analyzing the response of biological cells to the hemodynamic wall shear stress fields generated by the impinging flows found at arterial bifurcations [6, 7]. Here, we build on this work and design an in vitro flow chamber that can be used to reproduce specific magnitudes of wall shear stress (WSS) and gradients of wall shear stress. Particular attention is given to reproducing spatial distributions of these functions that have been shown to induce pre-aneurysmal changes in vivo [38]. We introduce a measure of the gradient of the wall shear stress vector (WSSVG) which is appropriate for complex 3D flows and reduces to expected measures in simple 2D flows. The WSSVG is a scalar invariant and is therefore appropriate for use in constitutive equations for vessel remodeling in response to hemodynamic loads [34, 35].

Keywords Intracranial aneurysm · Wall shear stress gradient · Flow chamber · Bifurcation

A.M. Robertson (✉)
Department of Mechanical Engineering and Materials Science, McGowan Institute for Regenerative Medicine, Center for Vascular Remodeling and Regeneration (CVRR); University of Pittsburgh, Pittsburgh, PA 15261, USA
e-mail: rbertson@pitt.edu

R. Rannacher, A. Sequeira (eds.), *Advances in Mathematical Fluid Mechanics*, 631
DOI 10.1007/978-3-642-04068-9_35, © Springer-Verlag Berlin Heidelberg 2010

1 Introduction

Due to the broad audience of this special volume, we begin this manuscript with a general introduction and motivation for this work. The arterial system is in some sense an optimized network of vessels [40]. In particular, it appears that the vasculature is designed to maintain the wall shear stress in vessels in a specific range, e.g. [15]. This is reflected in both the geometry of the vasculature and also in its ability to locally modify the vessel caliber through dilation and remodeling in response to changes in shear stress [23, 30, 50]. Throughout much of the arterial system, the velocity field is predominantly parallel to the vessel centerline. However, there are locations such as bifurcations, regions of sudden expansion and highly curved segments where the hemodynamic loading is far from this idealized flow, e.g. [26, 36]. These regions may display recirculation, flow impingement, acceleration/deceleration, and points of flow separation. In these areas, the magnitude and direction of the wall shear stress vector, $\underline{t}_s$, may change in space and time and be far from that associated with the nearly uni-directional flow found in straighter, more uniform arteries. For this reason, these flows are often referred to as "disturbed flows."

The fact that pathological changes to the vessel wall are correlated with these flows suggests the nature of the stress vector in these areas is outside the "optimal range" and is challenging for the vasculature. For example, intimal thickening is found to be correlated with regions of very low and oscillating wall shear stress often found in the carotid artery sinus, e.g. [27]. The destructive remodeling of the vessel wall in these regions appears to be a maladaptive response to hemodynamics in this region.

The general nature of the term "disturbed flows" is misleading. It is now understood that the endothelial cells (EC) which line our arteries can distinguish between some types of complex flows. Their response to altered $\underline{t}_s$ includes changes in cell shape and alignment, changes in activation of ion channels, intercellular signaling, gene expression changes at the level of transcription and protein synthesis (see, e.g. [2, 9, 16, 36, 41]). These local responses can trigger a cascade of large scale events such as vasodilation, and vessel remodeling.

Because of the importance of the EC in both the normal maintenance of the arterial wall as well as pathological changes associated with disease, numerous in vivo and in vitro studies have been directed at understanding the coupling between $\underline{t}_s$ and EC response. Various hemodynamic parameters have been introduced with the intent of replacing this complex vector function with scalar quantities that capture the most significant features of $\underline{t}_s$ for a given biomechanical response. One such parameter is the magnitude of $\underline{t}_s$ which is nearly uniformly accepted as an appropriate measure of $\underline{t}_s$. It is simply denoted as WSS.

Another hemodynamic feature of interest is the surface gradient of the wall shear stress. The choice of a scalar measure for this quantity is less clear. This is particularly true for curved surfaces where the spatial gradient of $\underline{t}_s$ has an out of plane contribution. A variety of scalar functions of the spatial gradient of $\underline{t}_s$ are used in the literature. Unfortunately, they are all denoted as WSSG, confounding comparison of results from different groups [5, 22, 25]. In most cases, a non-negative quantity is used, which cannot capture the dependence of the biological response on the sign of the gradient. In Sect. 2.1.1, we introduce a new measure of the wall shear stress gradient denoted as WSSVG rather than WSSG to emphasize that it is dependent on the gradient of the wall shear stress vector not the gradient of the WSS. This parameter has a number of advantages. It is appropriate for complex 3D flows and reduces to expected measures in simple 2D flows. The sign of WSSVG reflects the increasing and decreasing nature of $\underline{t}_s$. In addition, this measure is a scalar invariant of a second order tensor, so will be appropriate for use in constitutive equations for vessel remodeling in response to hemodynamic loads (e.g. [34, 35]).

There is substantial evidence to support the hypothesis that hemodynamics also play an important role in the initiation and development of intracranial aneurysms (ICA), (see, e.g. [14, 19, 20, 24, 44, 45]). An ICA is a pathological condition of cerebral arteries characterized by degeneration of the internal elastic lamina (IEL) and media, accompanied by local enlargements of the arterial wall, typically into a saccular shape. Cerebral aneurysms are predominantly found at the apices of bifurcations and outer bends of highly curved vessels in or near the circle of Willis, a network of vessels at the base of the brain. At both these locations, the blood impinges on the arterial wall where it is redirected with strong spatial variations in $\underline{t}_s$ downstream of the impingement point.

Earlier computational work suggested that the impulse of the incoming flow on the apex region could directly damage even healthy arterial walls [11]. It was later shown that the results supporting this conjecture were unphysical due to the use of perfectly sharp corners in the study [18]. The local increase in pressure at the apex is on the order of a few mmHg, much smaller than the normal variation in pressure throughout the vasculature [6]. Since cerebral aneurysms can form in humans in the absence of hypertension, we conjecture the role of elevated hemodynamic pressures in aneurysm formation is to hasten mechanical damage and ultimate failure of an IEL previously weakened by biochemical factors. The magnitude and spatial distribution of $\underline{t}_s$ at the apex of the bifurcation is drastically different from the seemingly desired distribution of more uniform flow. It has been conjectured that some aspect of $\underline{t}_s$ at the apex of the bifurcation initiates a cascade of biochemical activities that lead to the degradation of the IEL and media, rather than directly damaging the wall. For example, the character of $\underline{t}_s$ may lead to an imbalance in the production of enzymes responsible for natural remodeling and turnover of the extracellular matrix.

Motivated by diseases such as atherosclerosis as well as the frequent onset of intimal hyperplasia following bypass surgery, numerous in vitro and in vivo studies have been performed to explore the role of WSS and WSSVG in pathological changes to the arterial wall (e.g. [5, 29, 41]). While some in vitro chambers are designed to isolate the effect of specific parameters, others attempt to reproduce a specific "disturbed" flow found in vivo. For example, parallel plate and cone-and-plate flow chambers have been used to study the role of WSS under conditions for which there is no spatial or temporal gradient in $\underline{t}_s$. A backward facing step was introduced into these chambers to recreate the recirculating flow associated with intimal hyperplasia in vivo [10], including a reattachment point and regions of deaccelerating and accelerating flow. DePaola et al. appear to be the first to conjecture that endothelial cells may be sensitive to the gradient of $\underline{t}_s$ [10].

Recent in vivo work suggests both the WSS and the WSSVG play an important role in aneurysm initiation. Significantly, the sign of the gradient in $\underline{t}_s$ has been reported to be important for pre-aneurysmal changes [39]. However, the chambers designed for atherosclerosis do not reproduce the salient hemodynamic features found at the apices of bifurcations where aneurysms tend to form. In particular, the WSS field downstream of the stagnation point is monotonic and the surface gradient of $\underline{t}_s$ is much smaller than that found at the apex of bifurcations. There is a pressing need for an in vitro flow chamber which reproduces the WSS and WSSVG fields associated with aneurysm formation in vivo.

An in vitro T-chamber for studies of cellular response to apex flows was first introduced by Robertson et al. [6, 7]. This chamber well approximates the WSS field found in idealized human cerebral bifurcations and forms the starting place for the present work. In this work, we design a T-chamber which successfully reproduces specific profiles in both WSS and WSSVG found to be associated with pre-aneurysm changes in canine arterial bifurcations [38, 39].

2 Methods

2.1 Governing Equations

We perform numerical simulations in an idealized arterial bifurcation as well as in segments of an in vitro flow chamber. For both cases, the fluid is idealized as incompressible, homogeneous and linearly viscous (Newtonian) and the flow is modeled as steady and isothermal. The relevant governing equations are therefore the incompressibility condition and equation of linear momentum. Referred to rectangular Cartesian coordinates, x_i, the governing equations in the fluid domain, Ω, are

$$\left.\begin{aligned} v_{i,i} &= 0, \\ \varrho\, v_{i,j} v_j &= -\,p_{,i} + \mu\, v_{i,jj}, \end{aligned}\right\} \text{ in } \Omega \qquad (1)$$

where v_i are the components of the velocity vector $\underline{v}$, p is the combined term representing the Lagrange multiplier arising from the incompressibility constraint (equivalent to the mechanical pressure) and the gravitational potential, μ is the constant viscosity and ϱ is the constant mass density. The notation $()_{,i}$ denotes $\partial()/\partial x_i$ and repeated indices imply summation over the values of the index $i = 1, 2, 3$.

The bounding surface of Ω is composed of rigid walls where the velocity is prescribed to be zero, as well as N inflow and outflow surfaces. The locations of these N surfaces are somewhat arbitrary, arising when we truncate the physical domain in order to make the computational problem tractable. The choice of boundary conditions on these surfaces is not unique from the physical or mathematical perspective.

We will specify the velocity on sur
surfaces denoted as Γ_α where $\alpha \in$ [
and the corresponding conditions are
below for particular simulations. The

$$t'_i \equiv (-$$

where n_j are the components of the
cally reasonable and computationally
formulations to prescribe $\underline{t}'$ to be pa
from (2),

$$(-p\delta_{ij} + \mu v_{i,}$$

For a discussion of the implementa
for example [3], for a comparison of
ditions see [17], and for numerical an
condition, see [21]. More recently, G
of the system (1) for the case of ste
applied at all inflow and outflow surf
the unsteady problem with more gene
sion of physical anomalies arising w
the modified stress vector is specified

2.1.1 Flow Parameters: Wall Shea

In this section, we give a more prec
wall shear stress and wall shear stress
these quantities be physically meani
that they are scalar invariants. This la
used in constitutive equations for des
wall such at the model proposed in [

We now consider the fluid domai
wall), Fig. 1. Consider an arbitrary p
with unit normal $\underline{n}$ directed into the f
P is defined as

$$\underline{t}_s =$$

We would like the WSS to be a s
Since a scalar valued function of a
expressed as a function of its inner pr

$$\text{WSS} =$$

We will specify the velocity on surfaces $\bar{\Gamma}_\alpha$ and the modified stress vector $\underline{t}'$ on surfaces denoted as Γ_α where $\alpha \in [0, 1, 2, ..N-1]$. The choice of these surfaces and the corresponding conditions are problem specific and therefore will be given below for particular simulations. The modified stress vector is defined as

$$t_i' \equiv (-p\delta_{ij} + \mu v_{i,j})n_j \tag{2}$$

where n_j are the components of the outward normal to the surface Γ_α. It is physically reasonable and computationally straightforward in appropriately chosen FEM formulations to prescribe $\underline{t}'$ to be parallel to $\underline{n}$ on inlet and outlet surfaces, so that from (2),

$$(-p\delta_{ij} + \mu v_{i,j})n_j = Cn_i \qquad \text{on } \Gamma_\alpha. \tag{3}$$

For a discussion of the implementation of (3) using the finite element method see, for example [3], for a comparison of this condition with other inflow/outflow conditions see [17], and for numerical and some mathematical aspects of this boundary condition, see [21]. More recently, Galdi has addressed the mathematical properties of the system (1) for the case of steady and unsteady flows when condition (3) is applied at all inflow and outflow surfaces [13]. Kučera and Skalák have considered the unsteady problem with more general boundary conditions [28]. An early discussion of physical anomalies arising when the usual Cauchy stress vector rather than the modified stress vector is specified at outflow boundaries is given in [33].

2.1.1 Flow Parameters: Wall Shear Stress and Wall Shear Stress Gradient

In this section, we give a more precise meaning to the scalar quantities called the wall shear stress and wall shear stress gradient. The central considerations are (i) that these quantities be physically meaningful based on known biological data and (ii) that they are scalar invariants. This last point is important when these quantities are used in constitutive equations for destructive remodeling and damage of the arterial wall such at the model proposed in [34, 35].

We now consider the fluid domain to be surrounded by a solid domain Ω' (the wall), Fig. 1. Consider an arbitrary point P on the interface of these domains $\partial\Omega$ with unit normal $\underline{n}$ directed into the fluid domain. The wall shear stress vector, $\underline{t}_s$ at P is defined as

$$\underline{t}_s = \underline{t} - \underline{t} \cdot \underline{n}\,\underline{n}. \tag{4}$$

We would like the WSS to be a scalar function of $\underline{t}_s$ with dimensions of stress. Since a scalar valued function of a vector is invariant if and only if it can be expressed as a function of its inner product (e.g. [48]), the choice of WSS is clear,

$$\text{WSS} = |\underline{t}_s| = \sqrt{\underline{t}_s \cdot \underline{t}_s}. \tag{5}$$

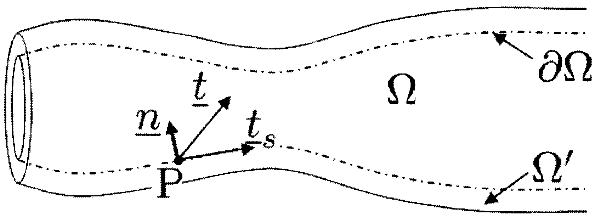

Fig. 1 Schematic of the vessel lumen and arterial wall

To our knowledge, there is only one work which does not use this definition [22].

We denote the spatial gradient of $\underline{t}_s$ with respect to surface coordinates as $\text{grad}_s\underline{t}_s$. For curved surfaces, $\text{grad}_s\underline{t}_s$ may not be a two dimensional tensor because the gradient of the surface base vectors may not lie on the surface. For example, consider the surface of a cylinder of circular cross section which is parameterized in terms of standard cylindrical components (θ, z). The $\text{grad}_s\underline{t}_s$ has an $\underline{e}_r \otimes \underline{e}_\theta$ component. We do not expect the biological cells to be sensitive to a purely geometric contribution of this kind, so we define a modified gradient of the wall shear stress vector as

$$\underline{G} = \text{grad}_s\underline{t}_s \; - \; \underline{n} \otimes (\underline{n} \cdot \text{grad}_s\underline{t}_s). \tag{6}$$

The quantity $\underline{G}$ is a two dimensional second order tensor with two principal invariants $\text{tr}(\underline{G})$ and $\det\underline{G}$, (e.g. [48]). Based on physical motivations elaborated on below, we define the *WSSVG* as,

$$\text{WSSVG} \; = \; \text{tr}\,\underline{G}. \tag{7}$$

We emphasize that WSSVG is an invariant of the gradient of the wall shear stress *vector* and not the gradient of the WSS. To avoid confusion, we do not use the notation WSSG. As we will see below, this is an important distinction and necessary to ensure the WSSVG captures the desired physical behavior.

To attain a clearer understanding of the physical meaning of these quantities, we consider the special case of 2D flow of an incompressible linearly viscous fluid over a flat surface. Using 2D rectangular coordinates (x_1, x_2), we define a solid boundary at $x_2 = 0$ with normal $\underline{e}_2$ into the fluid and consider velocity fields of the form, $\underline{v} = v_1(x_1, x_2)\underline{e}_1 + v_2(x_1, x_2)\underline{e}_2$. For such flows,

$$\text{2D flow :} \qquad \underline{t}_s \; = \; t_{s1}\underline{e}_1 \; = \; \mu\,\frac{\partial v_1}{\partial x_2}\underline{e}_1, \qquad \text{WSS} \; = \; \mu\left|\frac{\partial v_1}{\partial x_2}\right| \quad \text{at } x_2 = 0, \tag{8}$$

where we have made use of the no-slip condition. We see the WSS has the expected meaning of the magnitude of the viscous drag per unit area on the wall by the fluid. Furthermore, for these 2D flows,

$$\left[\text{grad}_s\underline{t}_s\right] \; = \; \Bigg[\; \mu$$

For flat plates, Eq. (6) simplifies
from (7) that,

2D flow :

The second principal invariant, d
the choice to use the trace invarian
ant is consistent with the desired dir
WSSVG is capable of distinguishing
its sign.

The difference in using the surfac
ent of the stress vector is clear if we
symmetric about the plane $x_1 = 0$. A
impinges on the plate with $v_1(-x_1, x$
The idealized 2D flow fields we consi
display this symmetry. From the pers
to flow of this type, we would like
try about the plane $x_1 = 0$ as well
$\text{WSSVG}(-x_1, x_2) = \text{WSSVG}(x_1, x_2$
function of x_1 and so would predict di
plane.

2.2 Flow in Idealized Bifurca

The T-chamber developed here is de
are typical of the apex region of ce
we briefly review the central feature
arterial bifurcations have been the su
in atherosclerosis and other vascular
concentrate on flow in the apex regi
are most likely to form.

Quantitative features of the bifurc
dependent on the bifurcation geometr
such idealized bifurcation model with
The bifurcation geometry was create
bifurcations [6, 49]. Approximate sol
ment method, implemented in ADIN
Analysis, Watertown, MA). The vel

$$\left[\,\mathrm{grad}_s \underline{t}_s\,\right] = \begin{bmatrix} \mu \dfrac{\partial^2 v_1}{\partial x_1 \partial x_2} & 0 \\ 0 & 0 \end{bmatrix}, \quad \text{at } x_2 = 0. \tag{9}$$

For flat plates, Eq. (6) simplifies to $\underline{G} = \mathrm{grad}_s \underline{t}_s$. It therefore follows directly from (7) that,

$$\text{2D flow}: \qquad \mathrm{WSSVG} = \mu \frac{\partial^2 v_1}{\partial x_1 \partial x_2}. \tag{10}$$

The second principal invariant, $\det(\mathrm{grad}_s \underline{t}_s)$, is zero for these 2D flows and so the choice to use the trace invariant is clear. A linear dependence on this invariant is consistent with the desired dimensions of WSSVG. It is clear from (10) that WSSVG is capable of distinguishing between increasing and decreasing t_{s1} through its sign.

The difference in using the surface gradient of WSS rather than the surface gradient of the stress vector is clear if we consider a special case of the 2D flow which is symmetric about the plane $x_1 = 0$. As an example, consider flows for which the fluid impinges on the plate with $v_1(-x_1, x_2) = -v_1(x_1, x_2)$ and $v_2(-x_1, x_2) = v_2(x_1, x_2)$. The idealized 2D flow fields we consider below for the apex region of the T-chamber display this symmetry. From the perspective of the response of the endothelial cells to flow of this type, we would like our "measured" WSSVG to display a symmetry about the plane $x_1 = 0$ as well. It follows directly from the result (10), that $\mathrm{WSSVG}(-x_1, x_2) = \mathrm{WSSVG}(x_1, x_2)$, as desired. Note that grad_s WSS is an odd function of x_1 and so would predict different behavior on either side of the symmetry plane.

2.2 Flow in Idealized Bifurcation Models

The T-chamber developed here is designed to reproduce shear stress fields which are typical of the apex region of cerebral arterial bifurcations. With this in mind, we briefly review the central features of such flows. Unsteady and steady flows in arterial bifurcations have been the subject of intense research, due to their relevance in atherosclerosis and other vascular diseases (see, e.g. [4, 18, 27, 51]). Here, we concentrate on flow in the apex region of bifurcations, where cerebral aneurysms are most likely to form.

Quantitative features of the bifurcation flow, such as the distribution of WSS, are dependent on the bifurcation geometry as well as the flow and fluid parameters. One such idealized bifurcation model with two planes of symmetry is shown in Fig. 2a, b. The bifurcation geometry was created using a parametric model for human cerebral bifurcations [6, 49]. Approximate solutions to (1) were obtained using the finite element method, implemented in ADINA (Automatic Dynamic Incremental Nonlinear Analysis, Watertown, MA). The velocity was prescribed to be zero on the lateral (rigid) walls. Boundary condition (3) was applied at the inlet and outlet surfaces with $C = 0$ on (Γ_1, Γ_2) and C set equal to a positive constant on Γ_0, chosen such that a Reynolds number (Re) of 255 was achieved, where

$$\mathrm{Re} = \varrho \bar{V} D/\mu, \tag{11}$$

D is the diameter at Γ_0 and $\bar{V} = 4Q/(\pi D^2)$ is the average velocity at the same location. For these studies, we choose parameters $\varrho = 1.05\,\mathrm{g/cm^3}$ and $\mu = 0.035\,\mathrm{g/(cm\,s)}$, $D = 4\,\mathrm{mm}$ and from (11), $\bar{V} = 21\,\mathrm{cm/s}$. The diameter of both daughter branches was set to 2.4 mm. These values are relevant for cerebral aneurysm formation.

As blood travels up the parent branch into the bifurcation region it impinges on the wall as it splits to flow into the two daughter branches, Fig. 2c. The blood then follows the curved geometry of the bifurcation into the daughter branches. The fluid close to the apex accelerates as it leaves the neighborhood of the impingement point, Fig. 2c. Displayed in Fig. 2d are the surface stress vectors $\underline{t}_s$ and iso-WSS contours

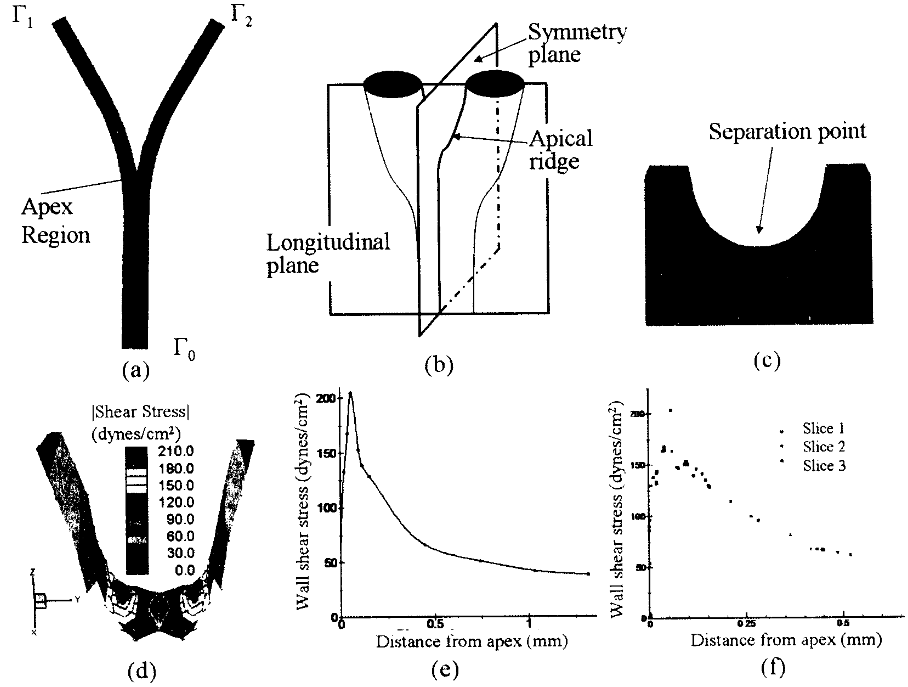

Fig. 2 Flow in an idealized bifurcation model. (**a**) Idealized geometry and computational domain Ω. (**b**) Schematic of cutting planes for bifurcation. (**c**) Velocity vectors in longitudinal plane of apex region. (**d**) Contours of the WSS (dynes/cm^2) with vectors $\underline{t}_s$ superimposed on iso-contours. (**e**) WSS along apical ridge defined by the intersection of apex and longitudinal plane. Distance is measured from impingement point. (**f**) WSS along apical ridge (slice 1) and planes parallel and separated by 0.04 and 0.08 mm from the longitudinal plane (slice 2 and 3, respectively)

for a saddle shaped region in the ne
along the apical ridge (formed by th
dinal plane) is plotted as a function
be seen in these two figures, WSS
impingement point to a local maxim

It is clear from Fig. 2d that the W
the bifurcation region. To assess thi
as slice 1 in Fig. 2f, corresponding
other curves is shown (labeled slice
curves formed by the intersection o
longitudinal plane, separated from it
If the stress field was perfectly two-
Though the maximum drops slightly
WSS can be seen to be close to tw
direction of vectors $\underline{t}_s$ are approxima
two-dimensionality is likely due to
the apex, are of opposite sign. Our
dimensionality in the neighborhood

Meng et al. [39] evaluated the re
to apical $\underline{t}_s$ fields. Artificial bifurcat
ments of common carotid arteries in
of these vessels, they obtained WSS
They divided the apex into three di
as Regions A,B,C. Region A displa
WSS > 20 dynes/cm^2, and positiv
20 dynes/cm^2 and negative WSSVG.
these regions. Significantly, in five of
changes including a thinned wall, d
endothelium. However, these same c
WSS magnitude was equally high th
that work, elevated WSS and positive
for aneurysm initiation.

2.3 Rationale Behind Design in the Bifurcation Chamb

The geometric features of the T-chaml
well approximates the WSS field four
This chamber forms the starting place
results just discussed, this T-chambe
features of both the WSS and WSSV
cellular function provide only a relati
it is desirable to build the chamber to r
as control fields. We introduce two co
WSS.

for a saddle shaped region in the neighborhood of the bifurcation. In Fig. 2e, WSS along the apical ridge (formed by the intersection of saddle region and the longitudinal plane) is plotted as a function of distance from the impingement point. As can be seen in these two figures, WSS is non-monotonic, increasing from zero at the impingement point to a local maximum value and then decreasing again.

It is clear from Fig. 2d that the WSS field is fairly two dimensional in nature in the bifurcation region. To assess this further, consider the WSS at points denoted as slice 1 in Fig. 2f, corresponding to the curve in Fig. 2e. The WSS along two other curves is shown (labeled slice 2 and 3) in Fig. 2f. These correspond to the curves formed by the intersection of the saddle region with planes parallel to the longitudinal plane, separated from it by distances of 0.04 and 0.08 mm, respectively. If the stress field was perfectly two-dimensional, these curves would be identical. Though the maximum drops slightly with distance from the longitudinal plane, the WSS can be seen to be close to two-dimensional in this region. Furthermore the direction of vectors $\underline{t}_s$ are approximately tangent to these planes, Fig. 2d. This near two-dimensionality is likely due to the fact that the principal radii of curvature at the apex, are of opposite sign. Our in vitro chamber makes use of this near two dimensionality in the neighborhood of the apex.

Meng et al. [39] evaluated the response of vascular tissue to sudden exposure to apical $\underline{t}_s$ fields. Artificial bifurcations were surgically created from native segments of common carotid arteries in dogs. Using CFD analysis in reconstructions of these vessels, they obtained WSS fields similar in form to those shown in Fig. 2e. They divided the apex into three distinct hemodynamic regions which we denote as Regions A,B,C. Region A displays WSS $\leq$ 20 dynes/cm^2, Region B displays WSS $>$ 20 dynes/cm^2, and positive WSSVG and Region C displays WSS $>$ 20 dynes/cm^2 and negative WSSVG. Distinct histological responses were found in these regions. Significantly, in five of six cases, Region B displayed pre-aneurysmal changes including a thinned wall, disrupted IEL, reduction in SMCs and loss of endothelium. However, these same changes were not found in region C where the WSS magnitude was equally high though the WSSVG was of a negative sign. In that work, elevated WSS and positive elevated WSSVG were found to be important for aneurysm initiation.

2.3 *Rationale Behind Design of Fluid Domain in the Bifurcation Chamber*

The geometric features of the T-chamber designed by Chung and collaborators [6, 7] well approximates the WSS field found in an idealized human cerebral bifurcations. This chamber forms the starting place of the present work. Motivated by the in vivo results just discussed, this T-chamber was modified to reproduce the quantitative features of both the WSS and WSSVG of the range reported in [39]. Many tests of cellular function provide only a relative measure (e.g. Western blotting, etc.) and so it is desirable to build the chamber to recreate both the bifurcation stress field as well as control fields. We introduce two control regions for exposure of cells to constant WSS.

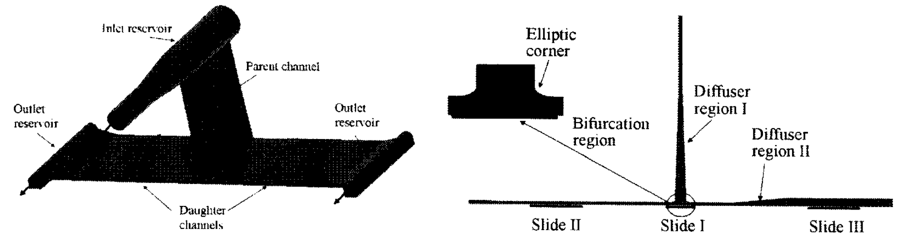

Fig. 3 Schematic of main features of fluid domain in flow chamber. (**a**) Entire 3D fluid domain (**b**) 2D cross section of fluid domain without reservoirs

A schematic of the general geometric features of the T-chamber are shown in Fig. 3, where the chamber orientation is inverted relative to the bifurcations shown in Fig. 2. Culture medium flows into the inlet reservoir, moves down the parent (vertical) channel, flows into the two daughter channels, into the outlet reservoirs and finally out of the chamber, Fig. 3a. Three separate slide regions are specified on the bottom plate: one in the region of the T-junction (slide I), two in control regions of constant WSS (slides II and III), Fig. 3b. Distinct slide banks are used to decrease contamination of the final biological cells from each test region with those from the transition regions. In addition, cross communication between cells in the different regions will be lessened.

Following [8], we define *Active Test Regions*, ATR-I, ATR-II, ATR-III, where the wall shear stress is within a chosen percentage of the desired 2D flow field for slides I, II and III. For ATR-II and ATR-III, the desired stress field will be a constant, corresponding to the solution for steady, fully developed, 2D, channel flow,

$$\tau_{fd_{2D}} = \frac{6Q\mu}{wh^2} = \frac{4V_o\mu}{h}, \tag{12}$$

where Q is the volumetric flow rate, V_o is the centerline (maximum) velocity, w is the channel width and h is the channel height. It follows from the exact analytic solution for 2D flow that $V_o = 3Q/(2hw)$. In the bifurcation slide, (slide I), the desired 2D field will correspond to the 2D bifurcation flow field, discussed in more detail below.

In summary, the T-chamber should meet the following criterion:

Design Criteria

1. A 2D WSS and WSSVG field is created on slide I which, with proper choice of flow rates, is relevant to (i) the apex of human cerebral arterial bifurcations and (ii) values for canine models in which pre-aneurysmal changes were reported.
2. Geometry of the flow domain creates nearly constant WSS fields on slides II and III. For example, supra-physiological WSS and physiological stress levels could be created in ATR-II and ATR-III, respectively.

3. The shear stress field should be
centage of the chamber. In parti
to provide sufficient quantities o
bifurcation region.
4. The thickness of the daughter ch
ance to obtain acceptable errors i
5. The flow chamber should be easi
6. The total volume of the chamber
cost of the testing fluid, chamber
byproducts.
7. The components of the chamber
ing sterilization.

A variety of perfusion fluids ar
approximately the same properties
to match the viscosity and density
$\mu = 0.032$ g/(cm s), $\varrho = 1.02$ g/cm^3
normal blood at 37°C at shear rates
latter values here.

It should be recalled, that the solu
a finite width. An analytic series solu
of rectangular cross section and car
The velocity is diminished in a boun
rate, the average velocity and WSS
layer in the finite channel comparec
The difference between the WSS ou
solution can be controlled through t
the geometries used here, this error i
estimate the WSS in slides II and III

3 T-Chamber Design: Analy

3.1 Fluid Domain

A 2D computational analysis was us
parameters in Fig. 4a such as the ch
bifurcation region. Next, the length c
region and the constant WSS regio
nearly fully developed when it reach
performed to design the inlet and c
fluid entering and exiting the chamb
a nearly 2D flow in the test region
comprehensive CFD study of the ful

3. The shear stress field should be approximately two dimensional in a large percentage of the chamber. In particular, the width of chamber should be chosen to provide sufficient quantities of cells for meaningful biological analysis in the bifurcation region.
4. The thickness of the daughter channels should be machined to sufficient tolerance to obtain acceptable errors in WSS and WSSVG.
5. The flow chamber should be easily assembled.
6. The total volume of the chamber fluid domain should be minimized to reduce the cost of the testing fluid, chamber body material and lessen the dilution of cellular byproducts.
7. The components of the chamber should be suitable for repeated autoclaving during sterilization.

A variety of perfusion fluids are used in the literature. In general, they have approximately the same properties as water. In other cases, an attempt is made to match the viscosity and density of blood. We take this latter approach and set $\mu = 0.032\,\mathrm{g/(cm\,s)}$, $\varrho = 1.02\,\mathrm{g/cm^3}$. These values are within the range reported for normal blood at 37°C at shear rates higher than $400\,\mathrm{s^{-1}}$, (e.g. [42]). We use these latter values here.

It should be recalled, that the solution (12) is for a 2D channel not a channel with a finite width. An analytic series solution exists for fully developed flow in channels of rectangular cross section and can be used to assess the error in using (12), [8]. The velocity is diminished in a boundary layer near the wall, so that for a given flow rate, the average velocity and WSS will generally be higher outside the boundary layer in the finite channel compared with the idealized 2D solution given in (12). The difference between the WSS outside this boundary layer and that in of the 2D solution can be controlled through the channel geometric ratio $\beta = h/w$, [8]. For the geometries used here, this error is less than 2% and so it is convenient to simply estimate the WSS in slides II and III using (12).

3 T-Chamber Design: Analysis and Results

3.1 Fluid Domain

A 2D computational analysis was used to select the relevant 2D chamber geometric parameters in Fig. 4a such as the channel heights (h_0, h_1, h_2) and the shape of the bifurcation region. Next, the length of the daughter channel between the bifurcation region and the constant WSS regions s_1 and s_2 was chosen to assure the flow is nearly fully developed when it reaches slides II and III. Finally a 3D analysis was performed to design the inlet and outlet reservoirs to diminish the effects of the fluid entering and exiting the chamber. These reservoirs are essential for obtaining a nearly 2D flow in the test regions. The final design was then checked using a comprehensive CFD study of the full 3D chamber.

3.1.1 Bifurcation Region

Criterion 1 was the central factor in the design of the bifurcation region. The 2D computational domain for these studies was composed of the parent channel, the bifurcation region and symmetric daughter branches of constant height, h_1, Fig. 4a. The modified stress vector $\underline{t}'$ was set to zero at the inlet and a parabolic profile with

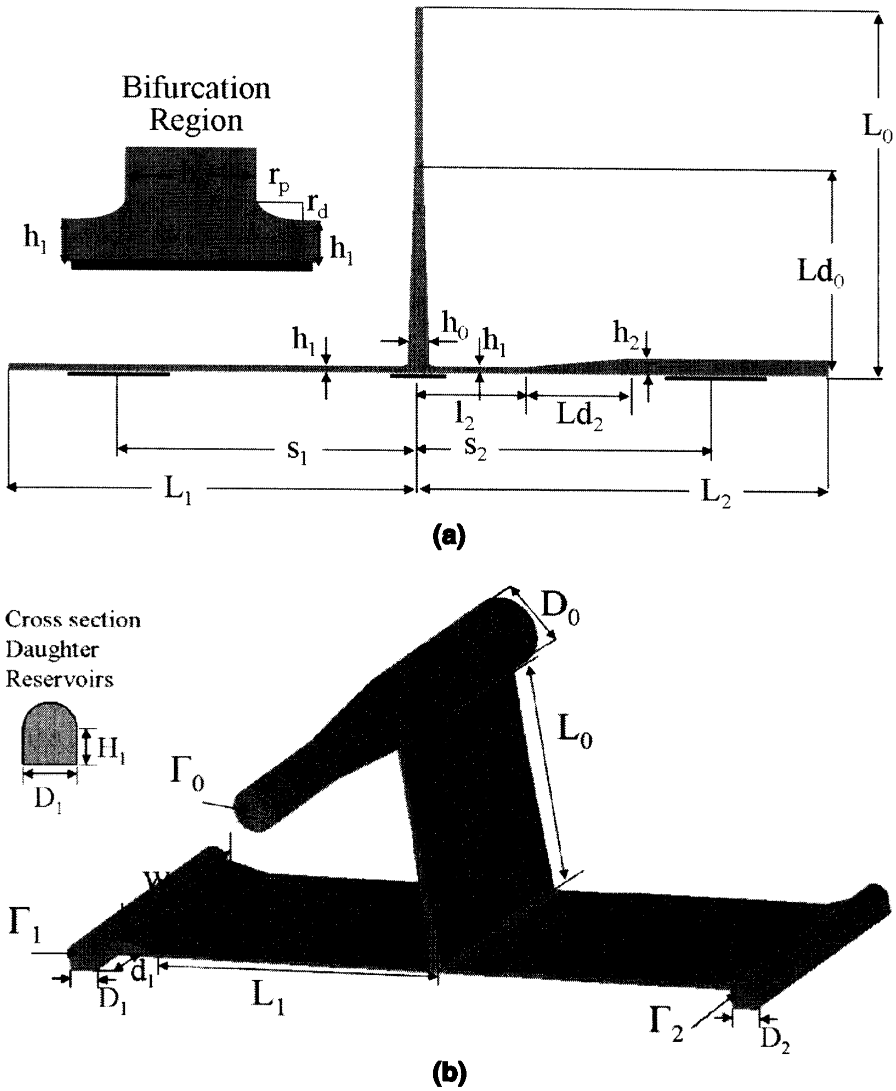

Fig. 4 Geometric parameters considered in chamber design. (**a**) 2D domain (no reservoirs), (**b**) full 3D domain

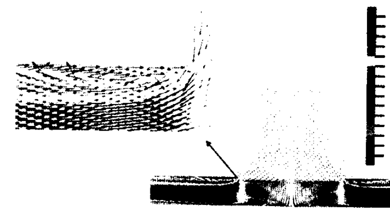

Fig. 5 Flow through a bifurcation with sl
bifurcation region with vortex seen dowr
centerline of bottom plate in region $x \in$
[1.0, 0.3, 0.3] mm

the desired flow rate was specified a
structured quadrilateral elements (b

The WSS distribution on slide
of the juncture between the parent
bifurcation) and the design of this
simple sharp corner has been used i
seen in Fig. 5a below and Fig. 1 of
vortices. The qualitative nature of th
Furthermore, these vortices can pote
ing additional errors in the imposed
Instabilities of this kind will not be

These vortices can be removed b
of an ellipse, Fig. 6. The elliptical g
$\varepsilon = \sqrt{(r_p^2 - r_d^2)/r_p^2}$, where r_p and r
The original chamber introduced in
distribution in the idealized bifurca
were quantitative differences in the
for the canine model, the maximum
bifurcation point, nearly twice the di
corner. By elongating the circular c
ables fixed, the location of the maxin
be seen Fig. 7 where 2D solutions
are shown for a circular corner ($\varepsilon =$
$\sqrt{3}/2$. Comparison of Figs. 7 and 8
on the WSS and WSSVG profiles. T
relatively insensitive to flowrate, whi
increasing Q. As can be seen in Fig.

design of the bifurcation region. The 2D
was composed of the parent channel, the
er branches of constant height, h_1, Fig. 4a.
ero at the inlet and a parabolic profile with

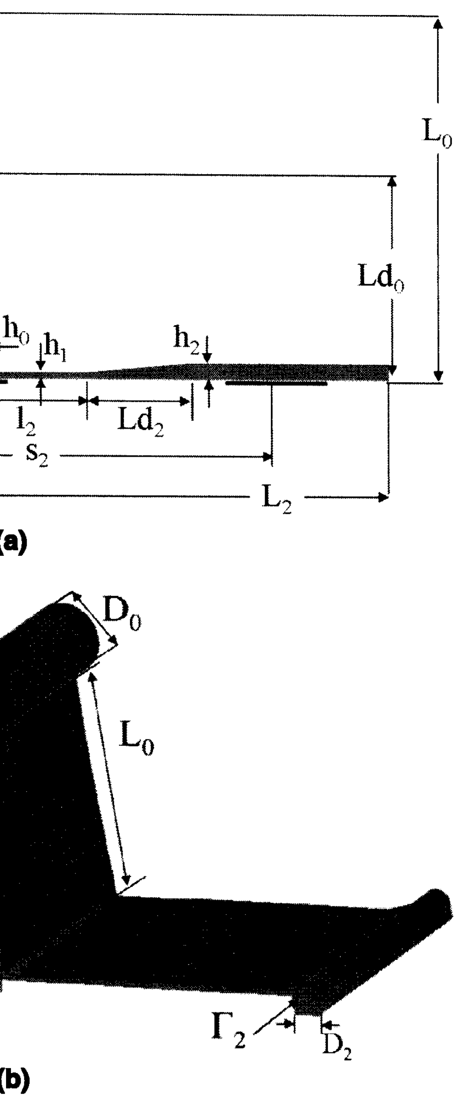

mber design. (**a**) 2D domain (no reservoirs), (**b**) full

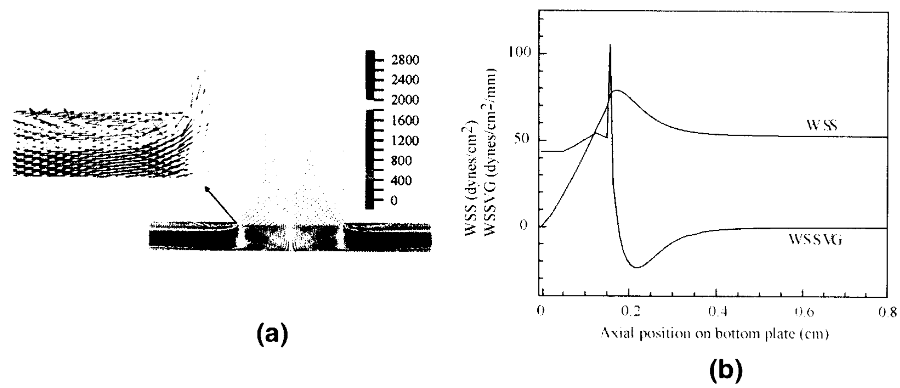

Fig. 5 Flow through a bifurcation with sharp corners (2D simulation). In (**a**), velocity vectors in bifurcation region with vortex seen downstream of sharp corner. In (**b**) WSS distribution along centerline of bottom plate in region $x \in [0.0, 0.8]$ cm. Here, $Q = 4518$ ml/min, $[h_0, h_1, h_2] = [1.0, 0.3, 0.3]$ mm

the desired flow rate was specified at each outlet. The FEM mesh was composed of structured quadrilateral elements (between 250 and 500K elements).

The WSS distribution on slide I was found to be quite sensitive to the shape of the juncture between the parent and daughter branches (the outer corner of the bifurcation) and the design of this region required the most intense evaluation. A simple sharp corner has been used in a recent T-chamber designs [47]. However, as seen in Fig. 5a below and Fig. 1 of [47], corners of this type can produce standing vortices. The qualitative nature of the WSSVG is altered by these vortices, Fig. 5b. Furthermore, these vortices can potentially be shed and washed downstream, creating additional errors in the imposed WSS and WSSVG fields on the bottom plate. Instabilities of this kind will not be captured in steady simulations.

These vortices can be removed by rounding the sharp corner to form a section of an ellipse, Fig. 6. The elliptical geometry can be characterized by the ellipticity, $\varepsilon = \sqrt{(r_p^2 - r_d^2)/r_p^2}$, where r_p and r_d are the half length of the major axis, Fig. 4a. The original chamber introduced in [6, 7], provided a good match with the WSS distribution in the idealized bifurcation using a circular corner ($\varepsilon = 0$), but there were quantitative differences in the WSS from those reported in [38]. In particular, for the canine model, the maximum in WSS (WSS_{max}) is found 2–3 mm from the bifurcation point, nearly twice the distance of that in the T–chamber with a circular corner. By elongating the circular corner (increasing ε), while holding other variables fixed, the location of the maximum in WSS shifts downstream. This effect can be seen Fig. 7 where 2D solutions for the WSS and WSSVG on the bottom plate are shown for a circular corner ($\varepsilon = 0$) and an elliptical corner with ε increased to $\sqrt{3}/2$. Comparison of Figs. 7 and 8 demonstrates the effect of increasing flowrate on the WSS and WSSVG profiles. The location where the WSSVG changes sign is relatively insensitive to flowrate, while both WSS_{max} and $WSSVG_{max}$ increase with increasing Q. As can be seen in Fig. 9, the WSS_{max} is quite sensitive to the channel

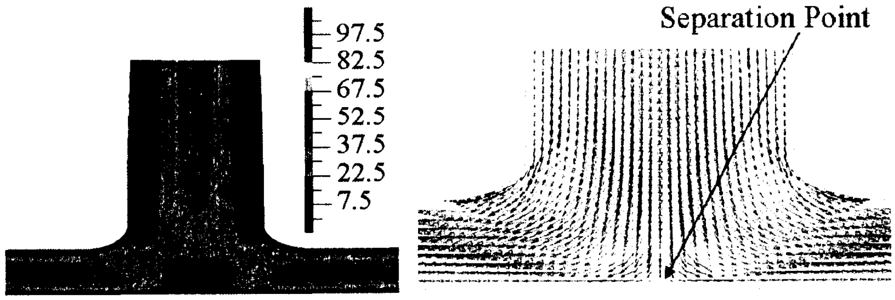

Fig. 6 Flow through a bifurcation with elliptical corner (2D simulation). In (**a**), magnified view of bifurcation with streamlines superimposed on iso-velocity contours (mm/s). In (**b**), magnified view of velocity vectors in bifurcation region. Here, $Q = 1333$ ml/min and geometric parameters are given in Table 1

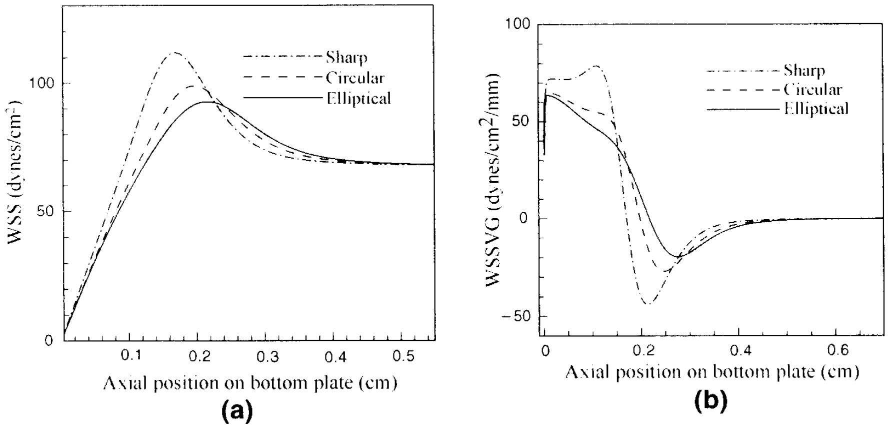

Fig. 7 Comparison of (**a**) WSS and (**b**) WSSVG on the *bottom plate* of T-chambers with elliptical, circular and sharp corners, (2D simulations) $Q = 1333$ ml/min, $\varepsilon = \sqrt{3}/2$, $R_c = 0.5$ mm, with all other geometric parameters given in Table 1

height of the daughter branch. As h_1 is narrowed from 0.8 to 0.4 mm for fixed h_0, the $\mathrm{WSS}_{\max}$ more than doubles with a very slight downstream shift in its location. It was found that by adding a slight taper to the channel upstream of the bifurcation, the magnitude and location of the $\mathrm{WSSVG}_{\max}$ could be easily controlled with little change in $\mathrm{WSS}_{\max}$, making it possible to closely match specific WSS and WSSVG profiles.

Using these trends as guidelines, it was possible to select ε, h_0, h_1 and the parent channel taper in such a away to obtain bifurcation WSS and WSSVG values that capture the main quantitative features of a given arterial bifurcation. For example, shown in Fig. 10 is a comparison between WSS and WSSVG profiles

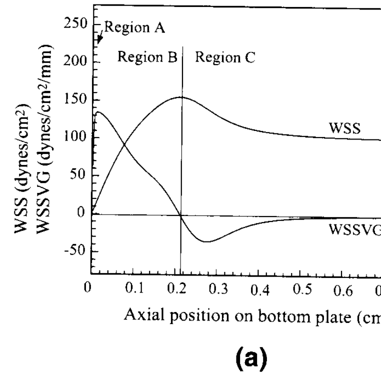

Fig. 8 WSS and WSSVG distribution alo
simulations) with elliptical outer bifurcat
other geometric parameters given in Table
(**b**) $Q = 2400$ ml/min. Region A is defin
dynes/cm^2 and positive WSSVG and Regi

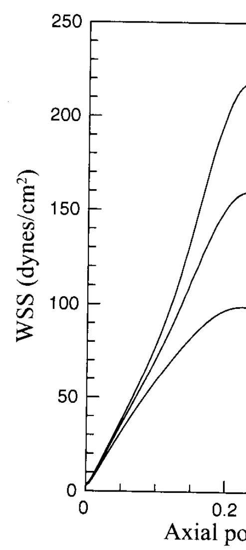

Fig. 9 WSS distribution along *centerlin*
[0.4, 0.6, 0.8] mm, (2D simulations) with e
All other geometric parameters are given i

for a representative canine data set f
designed to obtain a quantitative mat

3.1.2 Test Regions II and III

The chambers are designed to be run
ter branches. This ensures the flow

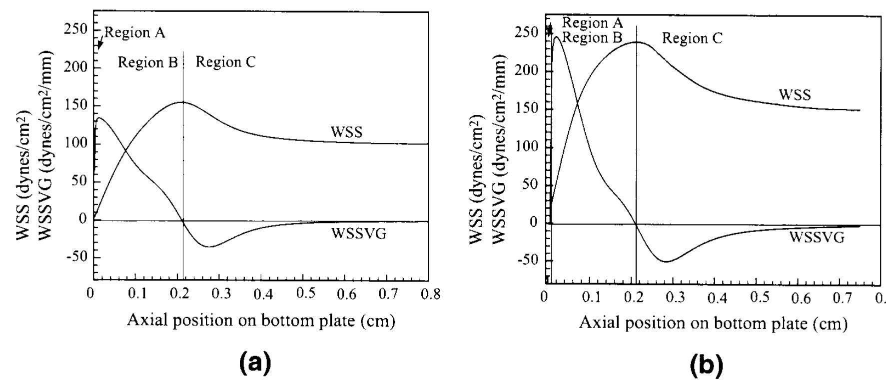

Fig. 8 WSS and WSSVG distribution along *centerline* of bottom plate in bifurcation region (2D simulations) with elliptical outer bifurcation $\varepsilon = \sqrt{3}/2$, $h_0, h_1, h_2 = [3.0, 0.8, 1.2]$ mm and all other geometric parameters given in Table 1. Two flowrates are considered: (**a**) $Q = 2000$ ml/min, (**b**) $Q = 2400$ ml/min. Region A is defined by WSS ≤ 20 dynes/cm^2, Region B by WSS > 20 dynes/cm^2 and positive WSSVG and Region C by WSS > 20 dynes/cm^2 and negative WSSVG

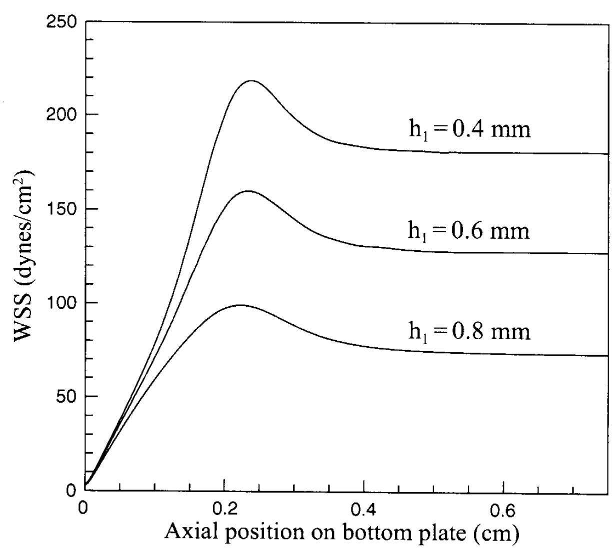

Fig. 9 WSS distribution along *centerline* of bottom plate in bifurcation region for $h_1 = [0.4, 0.6, 0.8]$ mm, (2D simulations) with elliptical outer bifurcation $\varepsilon = \sqrt{3}/2$, $Q = 1333$ ml/min. All other geometric parameters are given in Table 1

for a representative canine data set from [39] and results from a T-chamber model, designed to obtain a quantitative match of this data.

3.1.2 Test Regions II and III

The chambers are designed to be run with an equal flow split between the two daughter branches. This ensures the flow in the bifurcation region is nearly symmetric

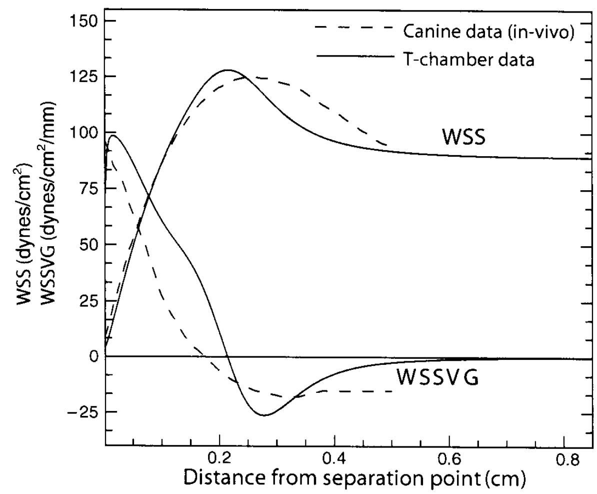

Fig. 10 WSS and WSSVG profiles in bifurcation region of canine model and T-chamber. T-chamber flowrate and geometry chosen to approximate maximum in WSS and WSSVG in canine data as well as qualitative shapes of curves. In T-chamber study $L_{d0} = 18$ mm and $Q = 1750$ ml/min, (2D simulations). All other geometric parameters are given in Table 1

about the plane $x = 0$. In this case, the flowrate in each daughter channel is $Q_d = Q/2$. The transition regions between slides I and the slides in the daughter branches are designed to achieve nearly fully developed flow prior to slides II and III. Assuming the flow is approximately 2D, the WSS on each daughter slide can then be calculated directly from (12). A 2D CFD analysis was performed to select the geometry of the diffuser and slide location that would guarantee the flow to be nearly fully developed on both slides. Values for the current chamber are shown in Table 1.

Table 1 Values (in mm) of geometric parameters for T-chamber, Fig. 4. The ellipticity (ε) is $\sqrt{3}/2$. The slide widths (in the flow direction) for slides I, II and III are 15, 25 and 25 mm, respectively

h_0	h_1	h_2	L_0	$L_1 = L_2$	w	l_2	Ld_0	Ld_2	$s_1 = s_2$	D_0	$D_1 = D_2$	$d_1 = d_2$
3.0	0.8	1.2	50	70	48	14	30	7.5	45	16	6	15

3.2 Reservoir Design

As discussed in detail in [8], the size of the ATR is influenced by the magnitude of the lateral wall effects as well as entrance and exit effects. While simply increasing the length of the chamber segments upstream of the test regions will generally lead to a more 2D flow it will also increase the volume of perfusion fluid. The cellular byproducts of the cells in the chamber are sometimes evaluated from samples of the perfusion fluid obtained during experiments [12]. By decreasing the volume of

fluid, the cost of the experiment ca
higher concentrations of these mate
Parametric studies were perform
and diffusers for the parent and da
for these studies consisted of the in
voir and the adjacent parent/daugh
was applied at the inlet/outlet of the
vector was set to zero at the outlet/i
to provide a large quantity of slides
slip cover and slide lengths.
The inlet reservoirs decreased th
ing and help to redistribute it across
to the 2D nature of the flow. The sh
its effectiveness [8]. Following [7, 8
flow perpendicular to the flow direc
inlet flow, a reservoir of circular c
provide a good balance between d
reservoir design was found to be v
flow entering the inlet reservoir the
nel needed to ensure the flow is ne
the iso-velocity (magnitude) contou
reservoir and parent channel. The c
reservoir. The diffuser effectively c
short distance downstream of the di

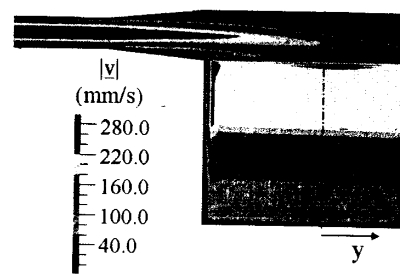

(a)

Fig. 11 Evaluation of transition to fully de
(**a**) iso-velocity contours in yz-plane (mm/
upstream of bifurcation slide ($x = 0$, z
[3.0, 0.8, 1.2] mm and all other geometric
show in Fig. 3

fluid, the cost of the experiment can be decreased and it will be possible to obtain higher concentrations of these materials.

Parametric studies were performed to design the shape and size of the reservoirs and diffusers for the parent and daughter channels. The 3D computational domain for these studies consisted of the inlet/exit to the reservoir, the inlet/daughter reservoir and the adjacent parent/daughter channel, Fig. 4b. A uniform velocity profile was applied at the inlet/outlet of the computational domain and the modified traction vector was set to zero at the outlet/inlet. The width of the channel was set to 48 mm to provide a large quantity of slides for cell culture while matching readily available slip cover and slide lengths.

The inlet reservoirs decreased the incoming momentum of the flow from the tubing and help to redistribute it across the width of the chamber, thereby contributing to the 2D nature of the flow. The shape of the reservoir has a significant impact on its effectiveness [8]. Following [7, 8], we chose cylindrical reservoirs with incoming flow perpendicular to the flow direction in the neighboring channel, Fig. 4b. For the inlet flow, a reservoir of circular cross section with $D_0 = 16$ mm was found to provide a good balance between damping effects and volume requirements. The reservoir design was found to be very effective at damping the momentum of the flow entering the inlet reservoir thereby diminishing the length of the parent channel needed to ensure the flow is nearly 2D in the test regions. Figure 11a displays the iso-velocity (magnitude) contours in the symmetry plane ($x = 0$) of the inlet reservoir and parent channel. The damping of the inlet jet can be seen within the reservoir. The diffuser effectively converts the incoming jet to a nearly 2D flow, a short distance downstream of the diffuser. There are two slight modifications in this

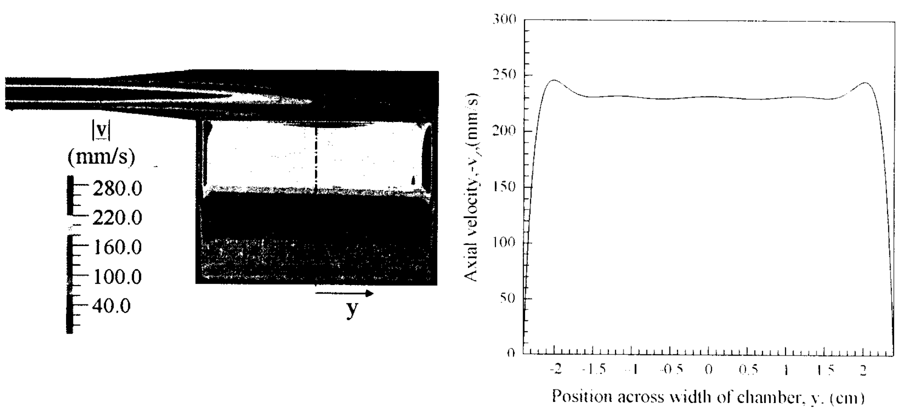

(a) (b)

Fig. 11 Evaluation of transition to fully developed flow in parent channel (3D simulations) with (**a**) iso-velocity contours in yz-plane (mm/s) and (**b**) axial velocity ($-v_z$) as a function of y just upstream of bifurcation slide ($x = 0$, $z = 36$ mm), with $Q = 1333$ ml/min, $[h_0, h_1, h_2] = [3.0, 0.8, 1.2]$ mm and all other geometric parameters are given in Table 1. Coordinate system show in Fig. 3

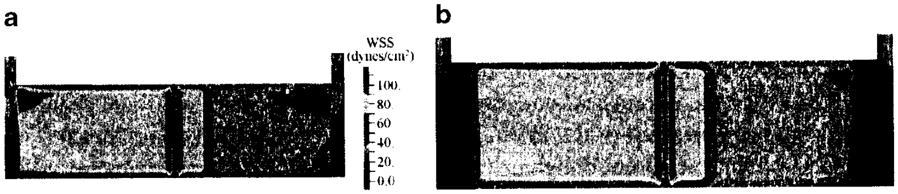

Fig. 12 WSS (dynes/cm^2) contours on *bottom surface* of flow domain, (3D simulation) for chamber (**a**) without diffusers and (**b**) with diffusers at outlet reservoirs. Geometric parameters are given in Table 1 and $Q = 2000$ ml/min

inlet reservoir design from that in [7, 8]. In the earlier chamber, a constant radius extension of the reservoir was used on both sides of the channel. Here, the constant radius inlet extension was replaced by a diffuser. The opposing extension on the inlet reservoir was found to have little impact on the flow and was removed in the current chamber.

The addition of two outlet diffusers upstream of the daughter reservoirs was found to significantly lessen the upstream influence of the reservoirs, Fig. 12. These reservoirs were designed independently from the parent reservoir and, for simplicity, were chosen to be identical. The cross section shape of is the union of a half circle of diameter D_1 and a rectangle of height H_1, Fig. 4b. The value of the geometric parameters used in the final chamber design are given in Table 1.

3.2.1 Methods of Decreasing Fluid Volume

The fluid domain can potentially be reduced in volume by decreasing the reservoir and channel volumes. Careful design of the reservoirs was used to diminish the entrance and exit lengths of the neighboring flow and therefore the lengths (and volume) of each channel. It was found that a region in the parent branch adjacent to the inlet reservoir could be narrowed to a thickness $h_p = 1/3h_0$ and then gradually expanded over a length Ld_0 to the desired value of h_0, Fig. 4a. Due to the gradual nature of the taper, these alteration to the parent channel had no measurable effect on the velocity field, WSS, or WSSVG in the bifurcation region. Values chosen for this chamber are given in Table 1. The total chamber volume is 25.8 ml.

3.3 Validation of T-Chamber Design

The design of the various sections of the chamber were performed for subsets of the entire final chamber geometry. It was therefore necessary to perform a 3D analysis for the full 3D chamber, including the inlet port and reservoirs. This corresponds to the complete computational domain shown in Fig. 4b using the geometric parameters in Table 1. A uniform velocity profile corresponding to the flowrate Q_d was prescribed at each of the outlets (Γ_1, Γ_2) to ensure equal flow division. The modified

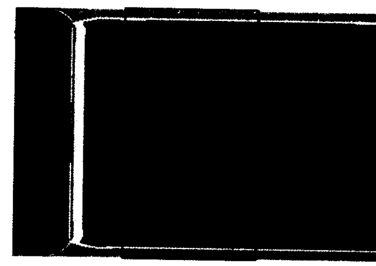

Slide II

Fig. 13 WSS (dynes/cm^2) contours on bo
(3D simulation). Geometric parameters ar

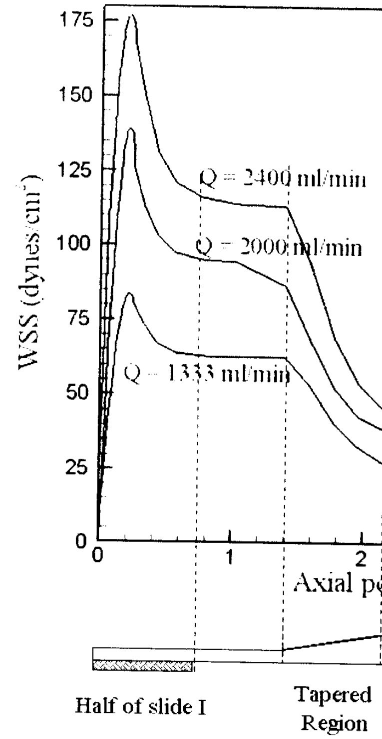

Fig. 14 WSS (dynes/cm^2) along centerline
ml/min with the geometry given in Table 1

traction vector was set to zero at the
hedral elements were used for these
are shown in Figs. 13 and 14.

The WSS on the bottom plate and
of ATR-II and III based on a criteri
2D value are drawn. The slide locat

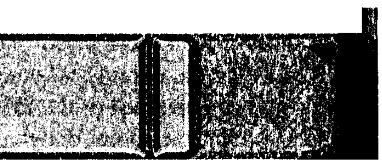

f flow domain, (3D simulation) for cham-
eservoirs. Geometric parameters are given

e earlier chamber, a constant radius
es of the channel. Here, the constant
ser. The opposing extension on the
on the flow and was removed in the

am of the daughter reservoirs was
nce of the reservoirs, Fig. 12. These
e parent reservoir and, for simplicity,
shape of is the union of a half circle
Fig. 4b. The value of the geometric
given in Table 1.

volume by decreasing the reservoir
eservoirs was used to diminish the
low and therefore the lengths (and
gion in the parent branch adjacent to
ness $h_p = 1/3h_0$ and then gradually
e of h_0, Fig. 4a. Due to the gradual
nt channel had no measurable effect
ifurcation region. Values chosen for
mber volume is 25.8 ml.

er were performed for subsets of the
necessary to perform a 3D analysis
and reservoirs. This corresponds to
Fig. 4b using the geometric param-
rresponding to the flowrate Q_d was
re equal flow division. The modified

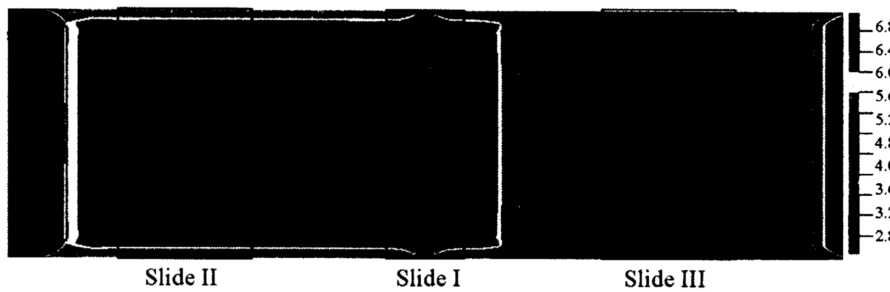

Fig. 13 WSS (dynes/cm^2) contours on bottom surface of flow domain, with labeled slide regions (3D simulation). Geometric parameters are given in Table 1 and $Q = 1333$ ml/min

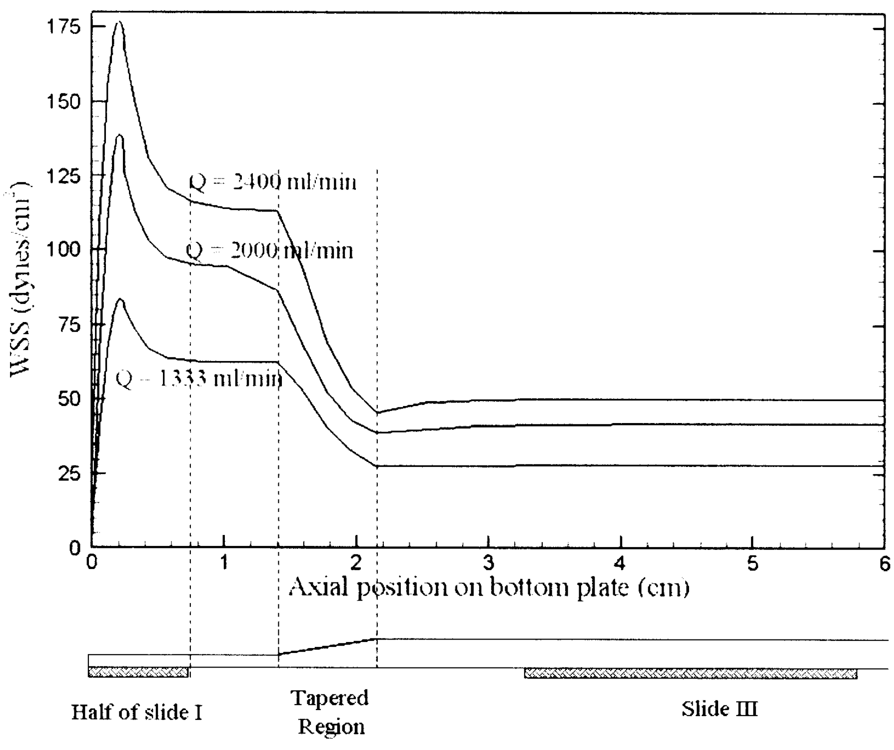

Fig. 14 WSS (dynes/cm^2) along centerline of *bottom plate* for flowrates, Q = [1333, 2000, 2400] ml/min with the geometry given in Table 1

traction vector was set to zero at the inlet, Γ_1. Approximately 70K structured hexahedral elements were used for these 3D studies. The results of this validation study are shown in Figs. 13 and 14.

The WSS on the bottom plate and reservoirs is shown in Fig. 13. The boundaries of ATR-II and III based on a criterion that the WSS be within 10% of the desired 2D value are drawn. The slide locations are drawn in solid lines with the lateral boundaries of the ATR drawn as dashed lines. The slide widths in the direction of flow are 15, 25 and 25 mm for slides I, II and III, respectively. For studies with $Q = 1333$ ml/min, the desired WSS values in ATR-II and ATR-III, are 70 dynes/cm^2 and 31 dynes/cm^2, respectively. Due to the no-slip condition at the lateral walls, there is a boundary layer where the WSS differs substantially from the 2D value. Conservatively, a domain excluding a 3 mm wide strip on each lateral side of the slides will satisfy the ATR criterion. Shown in Fig. 13 are the slide regions, all within the appropriate ATR. Necessarily, the slide must extend beyond the lateral boundaries of the ATR. This can be addressed either by removing these cells from the slide after testing and prior to genetic analysis, or by bounding the domain occupied by the cells (see, e.g. [37]). The effect of varying the flowrate on the WSS distribution on the bottom surface of the final flow chamber (geometric parameters in Table 1), is shown in Fig. 14. The three slides can be seen to be well located for all three flowrates tested.

When the chamber is placed within a flow loop for testing, the flow division can be controlled by downstream flow regulators. 2D CFD studies were performed to investigate the possible impact of imbalances in this split. Shown in Fig. 15 are results of a conservative study, in which a deviation of ±10% from the desired value was imposed. While the change in flow magnitude is reflected in the magnitude of the WSS, it is clear that the locations of both the impingement point and the maximum in WSS are nearly insensitive to an imbalance of this magnitude. Therefore, the interpretation of the three regions within slide I will not be jeopardized if an experimental error of this kind is introduced.

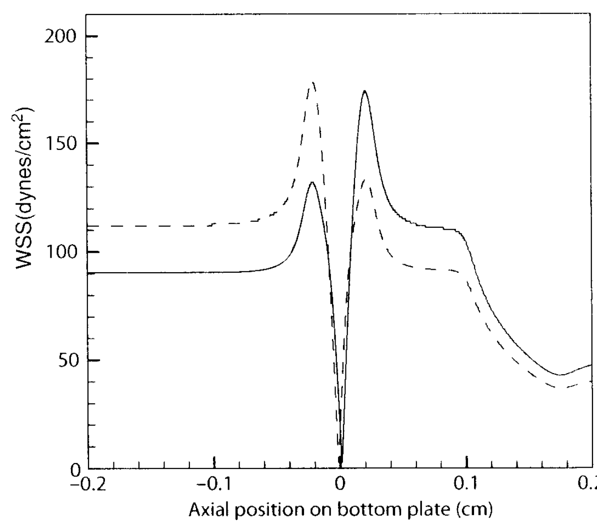

Fig. 15 Evaluation of the effect of a flow imbalance relative to a balanced flow $Q_1 = Q_2 = Q_n$. WSS along the bottom plate for imbalances $(Q_1, Q_2) = (1.1, 0.9)\ Q_n$ (*solid line*) and $(Q_1, Q_2) = (0.9, 1.1)\ Q_n$ (*dashed line*). Geometric parameters are given in Table 1 and $Q_n = 1000$ ml/min

4 Assembly Design and Ma

The 3D assembly design of the flo
Pro/ENGINEER Wildfire package
four plates which we denote as A
and an inlet adaptor. The breakdo
necessary for precise machining of
ratio ($w/h_0 = 16$, $w/h_{in} = 48$) a
and tapered). Machining of this cha
ing aspect of the manufacturing pr
and daughter reservoirs were mach
plates were cut to a tolerance of ±
Diecasting, NY). The inlet reservo
The slide slots were machined to a
side of layer D using CNC milling
Pittsburgh), Fig. 16a, b. These slots
change in height along the bottom
o-rings were used to seal all sectio
chosen to have 20–30% compressi
the mating pieces to properly seat
pins were used to assure proper alig
placed at opposite corners of the pa
Another critical aspect of the design

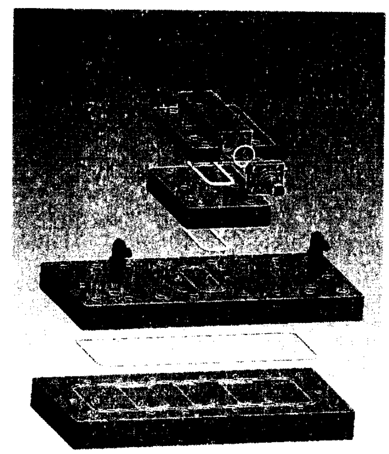

(a)

Fig. 16 (**a**) Exploded view of final T-cham
design of flow chamber. (**c**) Photograph of

4 Assembly Design and Manufacture

The 3D assembly design of the flow chamber is shown in Fig. 16a, generated using Pro/ENGINEER Wildfire package (PTC Inc). The entire chamber is composed of four plates which we denote as A, B, C, D from the top to bottom in Fig. 16(a) and an inlet adaptor. The breakdown of the upper chamber into three layers was necessary for precise machining of the parent channel which has a very high aspect ratio ($w/h_0 = 16$, $w/h_{in} = 48$) and two different cross sectional shapes (constant and tapered). Machining of this channel through layers A,B,C was the most demanding aspect of the manufacturing process. The daughter branches, daughter diffusers and daughter reservoirs were machined from the underside of Plate C. These three plates were cut to a tolerance of $\pm 0.002''$ (0.051 mm) using CNC milling (Atlantic Diecasting, NY). The inlet reservoir of diameter D_0 was drilled in the top piece. The slide slots were machined to a tolerance of $\pm 0.003''$ (0.076 mm) on the upper side of layer D using CNC milling (Swanson School of Engineering, University of Pittsburgh), Fig. 16a, b. These slots were custom cut to fit the slides to minimize any change in height along the bottom boundary of the fluid domain. Standard AS-568A o-rings were used to seal all sections of the T-chamber, Fig. 16a. The o-rings were chosen to have 20–30% compression to ensure a positive seal while still allowing the mating pieces to properly seat against each other. Precision ground alignment pins were used to assure proper alignment of the pieces during assembly. They were placed at opposite corners of the parts, which is sufficient for alignment on a plane. Another critical aspect of the design was the decision to avoid any glued parts which

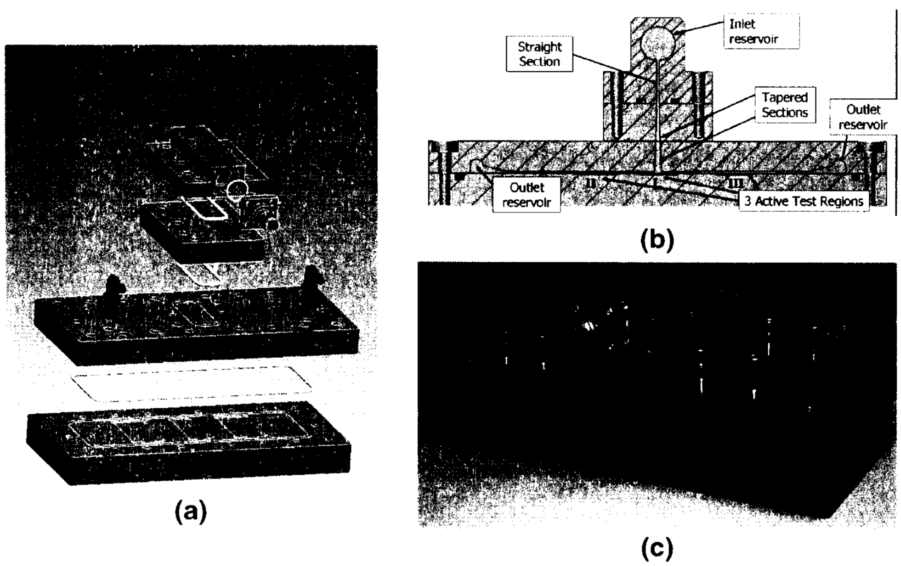

Fig. 16 (**a**) Exploded view of final T-chamber assembly design.(**b**) Cross section view of assembly design of flow chamber. (**c**) Photograph of manufactured T-chamber

could cause warping during autoclaving or potentially leak contaminants into the test chamber. Instead, the pieces were held together by stainless steel, standard hex, quarter 20 (1/4–20″) bolts (McMaster), Fig. 16c. Polysulfone was chosen for the chamber material due to its easy machinability and its ability to withstand autoclave conditions (120°C, 15 psi, 30 min). The final manufactured T-chamber is shown in Fig. 16c. Significantly, the tolerance for the channel heights h_0, h_1, h_2 are all set by the machining tolerances. This is in contrast to the use of gaskets to set the height in some channels.

5 Discussion

Cerebral aneurysms typically form at the apex region of arterial bifurcations. Hemodynamic stresses are believed to play an important role in the initiation of this pathology. Recent work in a canine model identified an association between pre-aneurysmal changes and a combination of elevated WSS and WSSVG in bifurcations formed from a naive vessel. This study was the first to connect in vivo histological changes with specific WSS and WSSVG profiles. The flow chamber designed here provides a tool for exploring these results in a controlled setting.

Most studies of endothelial cell response to mechanical stresses have been motivated by a desire to better understand the role of hemodynamics in the genesis and development of atherosclerosis. A number of researchers have developed in vitro chambers to evaluate the response of cellular components of the arterial wall (e.g. endothelial and smooth muscle cells) to homogeneous stress fields or recirculating flow fields of the type associated with atherosclerotic plaque formation. In early work in this field, DePaola et al., designed a step flow chamber which created a recirculating region [10]. At the edge of this region, the flow impinges on the wall and then separates – part of the flow circulating backward toward the step and the remainder moving downstream. However, the magnitude of the WSS and WSSVG fields in this flow are much smaller than those associated with aneurysm formation.

In this work, we have used parametric CFD studies to design a T-chamber capable of reproducing the qualitative and quantitative features of the WSS and WSSVG fields studied in [39]. The geometry of the flow domain was chosen using 2D and 3D CFD analyses. Building on earlier work for a parallel plate flow chamber [8] and the work in [6, 7], the magnitude of entrance and exit effects were controlled through careful design of chamber reservoirs. A full 3D analysis including all chambers was used to validate the final design. The chamber material was chosen for its easy machinability and its capability to withstand the high temperatures necessary for standard sterilization procedures.

To our knowledge, three previous T-chambers have been constructed [6, 8, 43, 46, 47]. The current chamber builds on that in [6, 8] with several principal changes. It is capable of generating a good approximating of both the WSS and WSSVG fields reported in [38, 39] and conjectured to lead to pre-aneurysmal changes. Secondly, an elliptical rather than circular corner is used at the bifurcation in order to shift the maximum in WSS further away from the impingement point. Thirdly, the chamber

is designed so that it does not requ
response. As in [6, 8], the height c
not set by the width of a gasket as

Several features distinguish this
use of inlet and outlet reservoirs to
ment of wall effects to less than 5%
formation in the bifurcation regio
for built in controls. Both T-cham
the test regions (approximately ind
due to inter-endothelial cell comm
humoral exchange and via gap junc
from the slides for later analysis,
data. The effects of the entrance f
flow in the slide regions. Fortunate
lowering the aspect ratio of the cha
a WSS less than 90% of the centerli
for fully developed flow in a chan
thickness to width ratio) is quite s
and parent branches with a corresp
of the chamber width. However, fo
[46, 47], the boundary layer on each
chamber width. The effect can be e
at the apex, (e.g. Fig. 2 of [47]). T
the inlet and outlet flow for the ch
large entrance and exit lengths whic
theory [1, 8]. The chamber used in
and outlets were omitted from the
design choice is not known. The co
to a rectangular channel in the par
have a significant downstream influ

Many tests of cell functionality
response. To address this issue, we
T-chamber. In the current chamber,
magnitudes. By switching out the
trols. Other control flows of interes
constant WSSVG flows.

The apex region of the current
erating vortices at the outer walls o
vortices will change the WSS prof
will be even more problematic if
downstream.

A variety of WSSG definitions ar
ing comparison of results from diffe
consider the $\underline{G} = \text{grad}_s \underline{t}_s$ to be of p
works, an orthogonal surface basis c

is designed so that it does not require any adhesives which could impact the cellular response. As in [6, 8], the height of the chamber is machined into the plates, and is not set by the width of a gasket as has been done in some earlier chambers.

Several features distinguish this T-chamber from that in [46, 47] including (i) the use of inlet and outlet reservoirs to diminish entrance and exit effects, (ii) confinement of wall effects to less than 5% of the chamber width, (iii) avoidance of vortex formation in the bifurcation region, and (iv) the use of three separate test regions for built in controls. Both T-chambers are directed at obtaining nearly 2D flow in the test regions (approximately independent of y, Fig. 3). This is particularly import due to inter-endothelial cell communication which is known to occur through both humoral exchange and via gap junctions. Furthermore, if the cells are to be removed from the slides for later analysis, the cells outside the ATR will contaminate the data. The effects of the entrance flow, exit flow and walls preclude complete 2D flow in the slide regions. Fortunately, the lateral wall effects can be diminished by lowering the aspect ratio of the chamber [8]. A boundary layer thickness defined by a WSS less than 90% of the centerline value can be estimated from the exact solution for fully developed flow in a channel [8]. For the current chamber, β (the channel thickness to width ratio) is quite small: 0.017, 0.025 and 0.0625 in the daughter and parent branches with a corresponding boundary layer thickness of 4.2% or less of the chamber width. However, for a parent value of $\beta = 0.15$ such as is found in [46, 47], the boundary layer on each side of the channel will rise to nearly 10% of the chamber width. The effect can be even more dramatic in the non-monotonic region at the apex, (e.g. Fig. 2 of [47]). The reservoirs significantly diminish the effect of the inlet and outlet flow for the chamber. The absence of reservoirs can result in large entrance and exit lengths which cannot be predicted by simple boundary layer theory [1, 8]. The chamber used in [46, 47] does not employ reservoirs. The inlets and outlets were omitted from the CFD analysis in [46, 47], so the impact of this design choice is not known. The connection of an inlet tube of circular cross section to a rectangular channel in the parent branch in their chamber will be expected to have a significant downstream influence.

Many tests of cell functionality provide only a relative measure of a particular response. To address this issue, we have included two control sections within the T-chamber. In the current chamber, the control flows are for a WSS of two different magnitudes. By switching out the bottom plate it is possible to change these controls. Other control flows of interest include flow over a backward facing step and constant WSSVG flows.

The apex region of the current chamber was carefully designed to avoid generating vortices at the outer walls of the bifurcation. Even for steady flows, these vortices will change the WSS profile on the bottom plate [46, 47]. Clearly this will be even more problematic if the vortices become unstable and are washed downstream.

A variety of WSSG definitions are used in the literature, unfortunately confounding comparison of results from different groups. As in this work, several researchers consider the $\underline{G} = \text{grad}_s \underline{t}_s$ to be of primary importance, (e.g. [5, 26, 32]). In these works, an orthogonal surface basis composed of a unit vector in the time averaged direction of $\underline{t}_s$ (for a cardiac cycle) and its perpendicular component are introduced. The WSSG is then defined as the square root of the sum of the squares of the diagonal elements of $\underline{G}$ using this basis. In contrast in [22], $\underline{G}$ is replaced with the 3D gradient of the full stress vector $\underline{t}$. For both these definitions, a non-negative quantity is used for the WSSG. In [25], the WSSG was approximated by the change in WSS divided by the change in axial position. In other works, particularly those with 2D flows in mind, the WSSG is not clearly defined. The variation in definitions may be one reason why groups have reported different correlations between biological markers for intimal hyperplasia and WSSG.

In this work, we have introduced a new measure of the gradient of the wall shear stress, denoted as WSSVG to distinguish it from these definitions of WSSG and to emphasize that it is not a measure of the gradient of WSS. We feel the WSSVG definition (7) has some advantages. It differentiates between increasing and decreasing shear stress through the sign of the WSSVG. It has been shown to be a scalar invariant of $\mathrm{grad}_s \underline{t}_s$ and it does not require calculation of the time averaged direction of WSS a priori. These last two points will become important if the WSSVG is to be incorporated into constitutive equations of the arterial wall, for example, to capture destructive remodeling during aneurysm formation [34, 35]. Furthermore, when the definition (7) is specialized to 2D flows over a flat surface, the sign of the gradient enters in a physically meaningful way.

In the future, it may be of interest to use this chamber for unsteady flows. In preliminary studies, we have found little difference between WSS and WSSVG results for steady simulations and the corresponding time averaged values for unsteady simulations using the same time averaged flow rates. It will also be useful to study the cellular response in real time. Modifications can be made to the bottom plate to achieve this objective.

Acknowledgments The authors would like to thank Andy Holmes of the Swanson Center for Product Innovation at the University of Pittsburgh for his valuable suggestions on the design and manufacture of the T-chamber. A number of undergraduates from the Department of Mechanical Engineering and Materials Science at the University of Pittsburgh have worked on an earlier version of the T-chamber as part of their senior design project and as undergraduate researchers. In particular, the authors would like to acknowledge John Barrow, Jason Larkin and David Remic [31]. A.M. Robertson would like to thank the Aachen Institute for Advanced Study in Computational Engineering Science (AICES) of the University of Aachen for a visiting professorship which she held during the period this paper was written.

References

1. Anderson, E., Falls, T., Sorkin, A., Tate, M.: The imperative for controlled mechanical stresses in unraveling cellular mechanisms of mechanotransduction. BioMed. Eng. OnLine **5**, 27 (2006) doi: 10.1186/1475-925X-5-27
2. Barbee, K., Davies, P., Lal, R.: Shear stress-induced reorganization of the surface topography of living endothelial cells imaged by atomic force microscopy. Circ. Res. **74**(1), 163–171 (1994)
3. Bathe, K.: *Finite Element Procedures*. Prentice Hall, Prentice (1996)

4. Berger, S.A., Lou, L.D.: Flows in ste
5. Buchanan, J.R., Kleinstreuer, C., hemodynamics and sites of altered junction. Atherosclerosis **143**(1), 27
6. Chung, B.J.: The study of blood flo on endothelial cell response to vess (2004)
7. Chung, B.J., Robertson, A.M.: A r to flow at arterial bifurcations. In: (BMES), p. 6P5.113. Nashville, Ten
8. Chung, B.J., Robertson, A.M., Pet chamber for investigation of endot 535–546 (2003). doi:10.1016/S004
9. Davies, P.F., Shi, C., Depaola, N., H origin of atherosclerosis: A spatial function. Ann. N.Y. Acad. Sci. **947**,
10. DePaola, N., Gimbrone, M., Davies shear stress gradients. [erratum appe Thromb. **12**(11), 1254–1257 (1992)
11. Foutrakis, G.N., Yonas, H., Sclabass cating arteries. Am. J. Neuroradiol.
12. Frangos, J.A., McIntire, L., Eskin, metabolism. Biotechnol. Bioeng. **32**
13. Galdi, G.P.: Mathematical problems Galdi, R. Rannacher, A.M. Robert *Analysis and Simulation*, Oberwolfa
14. Gao, L., Hoi, Y., Swartz, D.D., Kol tion at the basilar terminus induced b (2008)
15. Glagov, S., Zarins, C., Giddens, D. and perspectives gained from stu 1018–1031 (1988)
16. Goode, T., Davies, P., Reidy, M., B in situ by scanning electron micros **27**(2), 235–51 (1977)
17. Gresho, P.M.: Some current CFD is tions. Comput. Methods Appl. **87**, 2
18. Haljasmaa, I., Robertson, A.M., Ga stress and pressure in two-dimensio Appl. S. **11**(3), 499–520 (2001)
19. Hashimoto, N., Handa, H., Nagata, I. in rats: Part V. Relation of hemody Surg. Neurol. **13**(1), 41–45 (1980)
20. Hassler, O.: Experimental carotid li phological changes in the circle of V
21. Heywood, J.G., Rannacher, R., Tur ditions for the incompressible Navi 325–352 (1996)
22. Huo, Y., Guo, X., Kassab, G.S.: Th primary branches. Ann. Biomed. En
23. Kamiya, A., Togawa, T.: Adaptive re carotid artery. Am. J. Physiol. **239**, H
24. Kayembe, K., Sasahara, M., Hazam Willis. Stroke **15**, 846–850 (1984)

perpendicular component are introduced.
oot of the sum of the squares of the diag-
ntrast in [22], $\underline{G}$ is replaced with the 3D
these definitions, a non-negative quantity
was approximated by the change in WSS
other works, particularly those with 2D
defined. The variation in definitions may
different correlations between biological
G.

measure of the gradient of the wall shear
it from these definitions of WSSG and
e gradient of WSS. We feel the WSSVG
rentiates between increasing and decreas-
SSVG. It has been shown to be a scalar
calculation of the time averaged direction
become important if the WSSVG is to be
the arterial wall, for example, to capture
rmation [34, 35]. Furthermore, when the
ver a flat surface, the sign of the gradient

this chamber for unsteady flows. In pre-
rence between WSS and WSSVG results
ding time averaged values for unsteady
flow rates. It will also be useful to study
tions can be made to the bottom plate to

nank Andy Holmes of the Swanson Center for
for his valuable suggestions on the design and
rgraduates from the Department of Mechanical
ity of Pittsburgh have worked on an earlier ver-
gn project and as undergraduate researchers. In
John Barrow, Jason Larkin and David Remic
chen Institute for Advanced Study in Computa-
sity of Aachen for a visiting professorship which

he imperative for controlled mechanical stresses
anotransduction. BioMed. Eng. OnLine **5**, 27

duced reorganization of the surface topography
force microscopy. Circ. Res. **74**(1), 163–171

e Hall, Prentice (1996)

4. Berger, S.A., Lou, L.D.: Flows in stenotic vessels. Annu. Rev. Fluid Mech. **32**, 347–382 (2000)
5. Buchanan, J.R., Kleinstreuer, C., Truskey, G.A., Lei, M.: Relation between non-uniform hemodynamics and sites of altered permeability and lesion growth at the rabbit aorto-celiac junction. Atherosclerosis **143**(1), 27–40 (1999)
6. Chung, B.J.: The study of blood flow in arterial bifurcations: the influence of hemodynamics on endothelial cell response to vessel wall mechanics. Ph.D. thesis, University of Pittsburgh (2004)
7. Chung, B.J., Robertson, A.M.: A novel flow chamber to evaluate endothelial cell response to flow at arterial bifurcations. In: Annual meeting of the Biomedical Engineering Society (BMES), p. 6P5.113. Nashville, Tennessee (2003)
8. Chung, B.J., Robertson, A.M., Peters, D.G.: The numerical design of a parallel plate flow chamber for investigation of endothelial cell response to shear stress. Comput. Struct. **81**, 535–546 (2003). doi:10.1016/S0045-7949(02)00416-9
9. Davies, P.F., Shi, C., Depaola, N., Helmke, B.P., Polacek, D.C.: Hemodynamics and the focal origin of atherosclerosis: A spatial approach to endothelial structure, gene expression, and function. Ann. N.Y. Acad. Sci. **947**, 7–16; discussion 16–17 (2001)
10. DePaola, N., Gimbrone, M., Davies, P.F., Dewey, C.: Vascular endothelium responds to fluid shear stress gradients. [erratum appears in Arterioscler Thromb 1993 Mar;13(3):465]. Arterio. Thromb. **12**(11), 1254–1257 (1992)
11. Foutrakis, G.N., Yonas, H., Sclabassi, R.J.: Saccular aneurysm formation in curved and bifurcating arteries. Am. J. Neuroradiol. **20**(7), 1309–1317 (1999)
12. Frangos, J.A., McIntire, L., Eskin, S.G.: Shear stress induced stimulation of mammalian cell metabolism. Biotechnol. Bioeng. **32**, 1053–1060 (1988)
13. Galdi, G.P.: Mathematical problems in classical and non-newtonian fluid mechanics. In: G.P. Galdi, R. Rannacher, A.M. Robertson, S. Turek (eds.) *Hemodynamical Flows: Modeling, Analysis and Simulation*, Oberwolfach Seminars, vol. 37. Birkhäuser, Cambridge (2008)
14. Gao, L., Hoi, Y., Swartz, D.D., Kolega, J., Siddiqui, A., Meng, H.: Nascent aneurysm formation at the basilar terminus induced by hemodynamics. Stroke J. Cereb. Circ. **39**(7), 2085–2090 (2008)
15. Glagov, S., Zarins, C., Giddens, D., Ku, D.N.: Hemodynamics and atherosclerosis: insights and perspectives gained from studies of human arteries. Arch. Pathol. Lab. Med. **112**, 1018–1031 (1988)
16. Goode, T., Davies, P., Reidy, M., Bowyer, D.: Aortic endothelial cell morphology observed in situ by scanning electron microscopy during atherogenesis in the rabbit. Atherosclerosis **27**(2), 235–51 (1977)
17. Gresho, P.M.: Some current CFD issues relevant to the incompressible Navier-Stokes equations. Comput. Methods Appl. **87**, 201–252 (1991)
18. Haljasmaa, I., Robertson, A.M., Galdi, G.P.: On the effect of apex geomery on wall shear stress and pressure in two-dimensional models of arterial bifurcations. Math. Models Methods Appl. S. **11**(3), 499–520 (2001)
19. Hashimoto, N., Handa, H., Nagata, I., Hazama, F.: Experimentally induced cerebral aneurysms in rats: Part V. Relation of hemodynamics in the circle of Willis to formation of aneurysms. Surg. Neurol. **13**(1), 41–45 (1980)
20. Hassler, O.: Experimental carotid ligation followed by aneurysmal formation and other morphological changes in the circle of Willis. J. Neurosurg. **20**, 1–7 (1963)
21. Heywood, J.G., Rannacher, R., Turek, S.: Artificial boundaries and flux and pressure conditions for the incompressible Navier-Stokes equations. Int. J. Numer. Methods Fluids **22**, 325–352 (1996)
22. Huo, Y., Guo, X., Kassab, G.S.: The flow field along the entire length of mouse aorta and primary branches. Ann. Biomed. Eng. **36**(5), 685–699 (2008)
23. Kamiya, A., Togawa, T.: Adaptive regulation of wall shear stress to flow change in the canine carotid artery. Am. J. Physiol. **239**, H14–H21 (1980)
24. Kayembe, K., Sasahara, M., Hazama, F.: Cerebral aneurysms and variations in the circle of Willis. Stroke **15**, 846–850 (1984)

25. Keynton, R.S., Evancho, M.M., Sims, R.L., Rodway, N.V., Gobin, A., Rittgers, S.E.: Intimal hyperplasia and wall shear in arterial bypass graft distal anastomoses: An in vivo model study. J. Biomech. Eng. **123**(5), 464–473 (2001)
26. Kleinstreuer, C., Hyun, S., Buchanan, J.R., J, Longest, P.W., Archie J.P., J, Truskey, G.A.: Hemodynamic parameters and early intimal thickening in branching blood vessels. Crit. Rev. Biomed. Eng. **29**(1), 1–64 (2001)
27. Ku, D.N.: Blood flow in arteries. Annu. Rev. Fluid Mech. **29**(1), 399–434 (1997)
28. Kučera, P., Skalák, Z.: Local solutions to the Navier-Stokes equations with mixed boundary conditions. Acta Appl. Math. **54**(3), 275–288 (1998) 10.1023/A:1006185601807
29. LaMack, J.A., Himburg, H.A., Li, X.M., Friedman, M.H.: Interaction of wall shear stress magnitude and gradient in the prediction of arterial macromolecular permeability. Ann. Biomed. Eng. **33**(4), 457–464 (2005)
30. Langille, B.L.: Arterial remodeling: relation to hemodynamics. Can. J. Physiol. Pharmacol. **74**(7), 834–841 (1996)
31. Larkin, J., Barrow, J., Durka, M., Remic, D., Zeng, Z., Robertson, A.M.: Design of a flow chamber to explore the initiation and development of cerebral aneurysms. In: Annual Fall Meeting of the Biomedical Engineering Society (BMES). Los Angeles, CA (2007)
32. Lei, M., Archie, J.P., Kleinstreuer, C.: Computational design of a bypass graft that minimizes wall shear stress gradients in the region of the distal anastomosis. J. Vasc. Surg. **25**(4), 637–646 (1997)
33. Leone, J.M., Gresho, P.M.: Finite element simulations of steady, two-dimensional, viscous incompressible flow over a step. J. Comput. Phys. **41**(1), 167–191 (1981) doi: 10.1016/0021-9991(81)90086-3
34. Li, D., Robertson, A.M.: A structural multi-mechanism damage model for cerebral arterial tissue and its finite element implementation. Proceedings of the ASME 2008 Summer Bioengineering Conference (SBC-2008) (2008)
35. Li, D., Robertson, A.M.: A structural multi-mechanism damage model for cerebral arterial tissue. J. Biomech. Eng. **131**(10), 101013 (2009), doi:10.1115/1-3202559.
36. Malek, A.M., Izumo, S.: Mechanism of endothelial cell shape change and cytoskeletal remodeling in response to fluid shear stress. J. Cell Sci. **109**, 713–726 (1996)
37. McCann, J., Peterson, S., Plesniak, M., Webster, T., Haberstroh, K.: Non-uniform flow behavior in a parallel plate flow chamber alters endothelial cell responses. Ann. Biomed. Eng. **33**(3), 328–336 (2005) 10.1007/s10439-005-1735-9
38. Meng, H., Swartz, D.D., Wang, Z., Hoi, Y., Kolega, J., Metaxa, E.M., Szymanski, M.P., Yamamoto, J., Sauvageau, E., Levy, E.I.: A model system for mapping vascular responses to complex hemodynamics at arterial bifurcations in vivo. Neurosurgery **59**(5), 1094–1100; discussion 1100–1101 (2006)
39. Meng, H., Wang, Z., Hoi, Y., Gao, L., Metaxa, E., Swartz, D.D., Kolega, J.: Complex hemodynamics at the apex of an arterial bifurcation induces vascular remodeling resembling cerebral aneurysm initiation. Stroke **38**(6), 1924–1931 (2007)
40. Murray, C.D.: The physiological principle of minimum work. Proc. Natl. Acad. Sci. USA **12**(3), 207–214 (1926)
41. Nagel, T., Resnick, N., Dewey, C., Forbes, J., Gimbrone Michael, A., Jr.: Vascular endothelial cells respond to spatial gradients in fluid shear stress by enhanced activation of transcription factors. Arterio. Thromb. Vasc. Biol. **19**(8), 1825–1834 (1999)
42. Robertson, A.M., Sequeira, A., Kameneva, M.: Hemorheology. In: G.P. Galdi, R. Rannacher, A.M. Robertson, S. Turek (eds.) *Hemodynamical Flows: Modeling, Analysis and Simulation*, Oberwolfach Seminars, vol. 37. Birkhäuser, Cambridge (2008)
43. Sakamoto, N., Ohashi, T., Sato, M.: High shear stress induces production of matrix metalloproteinase in endothelial cells. In: Proceedings of the ASME 2008 Summer Bioengineering Conference (SBC2008). Marco Island, Florida (2008)
44. Sasaki, T., Kodama, N., Itokawa, H.: Aneurysm formation and rupture at the site of anastomosis following bypass surgery. J. Neurosurg. **85**, 500–502 (1996)

45. Sekhar, L.N., Heros, R.C.: Origin, rosurgery **8**, 248 –260 (1981)
46. Szymanski, M.: Endothelial cell bifurcation. Ph.d., State University
47. Szymanski, M., Metaxa, E., Meng ing flow mimicking the apex of an (2008)
48. Truesdell, C., Noll, W.: Non-linear *der Physik*, vol. III/3. Springer-Ve
49. Zakaria, H., Robertson, A.M., Ker bifurcations. Ann. Biomed. Eng. **3**
50. Zamir, M.: Optimality principles in
51. Zheng, L., Yang, W.: Biofluid dyn 455–493 (1992)

45. Sekhar, L.N., Heros, R.C.: Origin, growth, and rupture of saccular aneurysms: A review. Neurosurgery **8**, 248 –260 (1981)
46. Szymanski, M.: Endothelial cell layer subjected to flow mimickng the apex of an arterial bifurcation. Ph.d., State University of New York at Buffalo (2007)
47. Szymanski, M., Metaxa, E., Meng, H., Kolega, J.: Endothelial cell layer subjected to impinging flow mimicking the apex of an arterial bifurcation. Ann. Biomed. Eng. **36**(10), 1681–1689 (2008)
48. Truesdell, C., Noll, W.: Non-linear field theories of mechanics. In: S. Flugge (ed.) *Handbuch der Physik*, vol. III/3. Springer-Verlag, Berlin (1965)
49. Zakaria, H., Robertson, A.M., Kerber, C.: A parametric model for studies of flow in arterial bifurcations. Ann. Biomed. Eng. **36**(9), 1515–1530 (2008)
50. Zamir, M.: Optimality principles in arterial branching. J. Theor. Biol. **62**(1), 227–251 (1976)
51. Zheng, L., Yang, W.: Biofluid dynamics at arterial bifurcations. Crit. Rev. Biomed. Eng. **19**, 455–493 (1992)